Surface Reaction Near a Stagnation Point

By David A. Edwards

To measure rate constants while performing biomolecular interaction analysis (BIA), scientists often use resonant mirror devices such as the IAsys^{TM}. A full mathematical model of the IAsys^{TM} consists of a convection–diffusion equation in a closed well with a reacting surface at the bottom. The flow in the well is complex, but near the sensor, the qualitative nature of the reaction can be analyzed by reducing to stagnation point flow. The concentration of the reacting species in several cases is analyzed using singular perturbation techniques. Linear and nonlinear integral equations result from the analysis; explicit and series solutions are constructed for physically realizable cases. These solutions, which include the effects of transport on the reaction, provide improved estimates for the rate constants from raw IAsys^{TM} binding data.

1. Introduction

The accurate measurement of rate constants is key to the understanding of reactions in the biological and chemical sciences. If one or more of the reactants is not fixed in place, the effects of transport must also be considered. In particular, when both reactants are embedded in a flow, the resulting

Address for correspondence: Prof. D. A. Edwards, Department of Mathematical Sciences, University of Delaware, Newark, DE 19716-2553. E-mail: edwards@math.udel.edu

STUDIES IN APPLIED MATHEMATICS 105:1–29

Published by Blackwell Publishers, 350 Main Street, Malden, MA 02148, USA, and 108 Cowley Road, Oxford, OX4 1JF, UK.

system has been well studied (for example, see the classical textbook [1]). However, there have been fewer studies of the case when one of the reactants is embedded on a surface. In an industrial setting, such systems occur when one is trying to produce a reaction on a thin film—a so-called chemical vapor deposition (CVD) process [2–5]. In addition, gaseous components diffuse through highly porous catalysts to react on "active sites" in fixed-bed reactors [6]. Purification processes also utilize reactants embedded in pipe walls [7].

In the biological realm, such surface–volume reactions are also important. For example, DNA–protein interactions in these geometries (in particular, on the outside of a helical strip [8]) is a prime factor in gene expression [7]. Signaling and adapter molecules in the cytoplasm interact with the cytoplasmic tails of receptors embedded in the cellular plasma membrane [9]. Immunoglobulins are transmitted from mother to newborn *via* mother's milk through the mechanism of binding to receptors on intestinal epithelial cells [10].

Resonant mirror technology allows the measurement of rate constants in such surface–volume reactions; for a detailed introduction to the technology, see [11]. A schematic of the IAsys^{TM}, one popular measurement device, is shown in Figure 1. One reactant (the analyte) is placed in solution in the well, shown at right. The solution level is roughly 2 mm below the top of the well, as shown. In general, the volume of fluid considered is between 50 and 200 μL [12, 13]. The other reactant (the receptor) is embedded in a sensor surface at the bottom of the well, indicated with dark shading at the figure at left, which is a bottom view. The solution is agitated using a vibrostirrer that has an elliptical annular cross section, indicated with light shading. The center elliptical hole is 1 mm in the short direction. The stirrer oscillates at 140 cycles/s in the direction shown at up to 0.5-mm amplitude. The amplitude of the oscillation can be varied, and usually is set at around 85% of maximum [14].

As the reaction proceeds, a polarized light beam reflects off the sensor surface and passes to a detector. Refractive changes caused by the binding of the reactants are then averaged over the sensor surface to provide real-time measurement of the bound-state concentration [7, 15].

To simplify the analysis, many authors decouple the reaction kinetics from the transport dynamics [5, 16]. When one does so, the equations that result are simple first-order ODEs [17]. By separating these effects, these authors assume that the concentration of the analyte is uniform near the sensor surface. This is equivalent to assuming that reaction and transport occur on disparate time scales, so replacement analyte can be brought to the sensor surface more quickly than the reaction can use it up. Unfortunately, this decoupling occurs only when the parameter values are in certain ranges [15, 18].

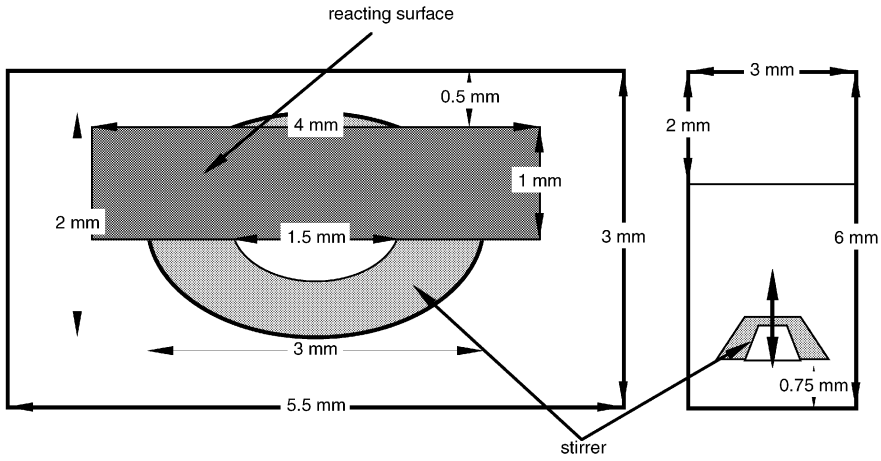

Figure 1. IAsys^{TM} device, bottom and side view.

Transport effects must be included in the analysis if the parameters do not fall in these ranges [19], and there are several ways to incorporate these effects [20]. Some authors prefer to introduce a new "mass transfer coefficient" to account for diffusive effects rather than modeling the full transport-reaction system [15, 21]. The expressions for these mass transfer coefficients may be directly derived from the full system of equations [8, 22].

In this article, we present a simplified model for the flow in the IAsys^{TM} device—stagnation point flow. This model for the flow will then allow us to pose the problem as an analytically solvable convection–diffusion system for the analyte $\tilde{C}$ with a reaction at the sensor surface. Because of the peculiar nature of the stagnation flow, an exact solution may be found when the initial density of receptor sites $\tilde{B}_{\mathrm{i}}$ is uniform across the sensor surface. The solution depends critically on the *Damköhler number* Da, which measures the ratio of the time scales of transport to reaction.

It is most often the case that $\tilde{B}_{\mathrm{i}}$ is, indeed, uniform. However, examination of the case where it is not, in addition to being interesting in its own right, illustrates techniques that can be used to solve the system with more complicated flow patterns. Using Da as a small parameter, we construct the first-order correction to the reaction-limited case caused by small transport effects. The solution thus obtained is in the form of a Mellin convolution, but can be solved explicitly for analytic $\tilde{B}_{\mathrm{i}}$.

The regular perturbation expansion in Da shows classic signs of secularity as $\tilde{t} \to \infty$. However, the resulting amplitude equation in a classic multiple-scale expansion cannot be solved explicitly. Last, we make some remarks on the case where $\tilde{B}_{\mathrm{i}}$ is not uniform and $\mathrm{Da} = O(1)$. In this case, a nonlinear in-

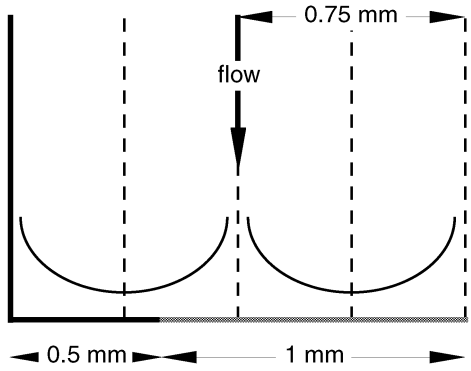

Figure 2. First idealization of IAsys^{TM} device.

tegral equation results, similar to the one in [18]. However, such an equation can be solved numerically [23].

2. The flow

From our discussion in section 1, it is clear that the flow in the IAsys^{TM} will be very complicated. The first question to consider is whether the flow remains laminar or becomes turbulent. Fortunately, the Reynolds number Re for the system is around 300 (for estimates of all the relevant parameters, see the Appendix). This value of Re implies bulk flow that can be treated as inviscid, but still laminar. Because the concentration of the bound state is averaged over the entire sensor surface (which is quite long compared to its width), we reduce the problem to two dimensions by taking a slice along the width of the device. In addition, we model the oscillating stirrer as a jet. This simplification, although at first glance severe, will be more fully justified later. Moreover, this simplification allows us to use potential theory for the bulk flow, thus yielding a tractable problem.

The system that results is shown in Figure 2. We model the stirrer as centered in the device, thereby imposing symmetry about the centerline, shown as the dashed line at the right of the figure. The reacting surface is shown shaded, not black on the bottom of the figure. Although the geometry in Figure 2 is simpler, there is a serious drawback for basic analytical solution methods. In particular, the ligand that participates in the reaction resides in an unstirred layer (thinner than the viscous layer) where diffusion and convection share dominance. Hence, we must know the flow inside the viscous boundary layer. In the geometry shown in Figure 2, the flow in the inner core will not allow a simple boundary-layer solution.

Therefore, for a first attempt at modeling, we use an even simpler geometry, shown in Figure 3. We model the flow as stagnation point flow. Because

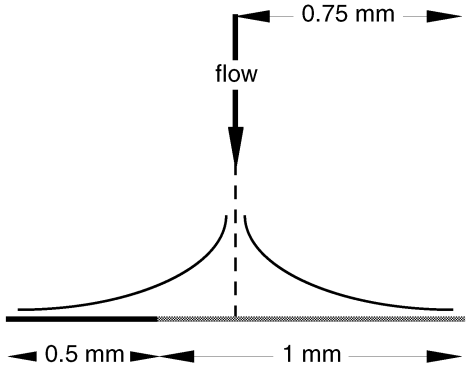

Figure 3. Second idealization of IAsys^{TM} device.

a relatively simple solution holds for the flow in the viscous boundary layer for this case, we can explicitly obtain a solution that contains many of the salient features of the over-all flow. In particular, we note that in Figures 2 and 3, as well as in the real system in Figure 1, a great deal of the sensor surface is in close proximity to a stagnation point. Therefore, we expect our solution to approximate closely the true solution, thus yielding reasonable estimates for the effects of transport in this device. (A very rough estimate for the size of the effects can also be obtained through dimensional analysis, as shown in section 3.3.)

We choose $\tilde{x}$ to be the direction along the sensor surface and $\tilde{y}$ to be the distance above the sensor surface. The stagnation point is taken as the origin, and, hence, we concern ourselves only with the region $\tilde{x} \geq 0$, $\tilde{y} \geq 0$. We take $\tilde{y} = H$ to be the rest position of the stirrer. Because the stirrer oscillates only in the $\tilde{y}$-direction, we have $\tilde{u}_{\tilde{y}}(0, H) = -V$. (In the oscillating case, the velocity is largest at the rest position.) For the length scale in the $\tilde{x}$-direction, we choose the distance L between the stirrer and the centerline, which is also the distance to the well wall. Thus, we introduce dimensionless variables by letting

$$\tilde{x} = Lx, \qquad \tilde{y} = Hy_{\mathrm{p}}, \qquad \tilde{u}_{\tilde{y}}(\tilde{x}, \tilde{y}) = Vu_y(x, y_{\mathrm{p}}). \tag{1}$$

To maintain a balance in the conservation of mass equation, we must scale the velocity in the $\tilde{x}$-direction as follows:

$$\tilde{u}_{\tilde{x}}(\tilde{x}, \tilde{y}) = \frac{VLu_x(x, y_{\mathrm{p}})}{H}.$$

Because the Reynolds number is large enough that we may use potential flow, we quote the well-known result for flow about a stagnation point [24]:

$$u_x = x, \quad u_y = -y_{\mathrm{p}}. \tag{2}$$

Although this solution satisfies the no-slip condition on u_y at the boundary $y_p = 0$, it does not satisfy the no-slip condition on u_x. Therefore, we must introduce the standard boundary-layer variables:

$$y_v = \mathrm{Re}^{1/2}\, y_p = \left(\frac{V}{H\nu}\right)^{1/2} \tilde{y}, \qquad u_x(x, y_p) = v_x(x, y_v), \tag{3a}$$

$$\mathrm{Re} = \frac{VH}{\nu}, \tag{3b}$$

where the subscript "v" refers to the viscous boundary layer. If we do so, the conservation of mass equation requires that

$$u_y(x, y_p) = \mathrm{Re}^{-1/2}\, v_y(x, y_v) \tag{4}$$

to obtain the balance

$$\frac{\partial v_x}{\partial x} + \frac{\partial v_y}{\partial y_v} = 0. \tag{5}$$

(Note that our scaling in (4) implies that the vertical velocity is very small.)

The remaining boundary layer equation is given in [25]:

$$v_x \frac{\partial v_x}{\partial x} + v_y \frac{\partial v_x}{\partial y_v} = u_x(x, 0)\frac{du_x}{dx}(x, 0) + \frac{1}{\mathrm{Re}\, r^2}\frac{\partial^2 v_x}{\partial x^2} + \frac{\partial^2 v_x}{\partial y_v^2}, \tag{6a}$$

$$v_x \frac{\partial v_x}{\partial x} + v_y \frac{\partial v_x}{\partial y_v} = x + \frac{\partial^2 v_x}{\partial y_v^2}, \qquad r = \frac{L}{H}, \tag{6b}$$

where we have used (2). Here r is related to the aspect ratio of the well. The relevant boundary and matching conditions are

$$v_x(x, 0) = 0, \qquad v_y(x, 0) = 0, \qquad v_x(x, \infty) = x, \qquad v_y(x, \infty) \sim -y_v.$$

Because of the condition on v_x as $y \to \infty$, we try a solution of the form

$$v_x = x f'(y_v) \tag{7a}$$

in (5), which yields

$$v_y = -f(y_v). \tag{7b}$$

Substituting (7) into (6b) and the boundary and matching conditions, we obtain

$$f''' - (f')^2 + ff'' + 1 = 0; \qquad f(0) = f'(0) = 0, \qquad f'(\infty) = 1.$$

This is a *Falkner–Skan* equation.

It will be shown that the transport layer is even thinner than the viscous layer, and, hence, we need the values of f only near $y_v = 0$. We note from solution profiles that f' is linear near $y = 0$. Therefore, if we call the constant of proportionality $2F$ (in other words, $F = f''(0)/2$), we have

$$f'(y_v) \sim 2Fy_v, \qquad f(y_v) = Fy_v^2, \qquad y_v \to 0. \tag{8}$$

Numerical calculations from Maple show that $F \approx 0.616$.

We point out that solutions of the form (7) exist for the boundary-layer equations (5) and (6a) only when $u_x(x, 0)$ is of the special form in (2). Although we are interested in the behavior of the flow only near $y_v = 0$, because of the matching conditions as $y_v \to \infty$, we cannot rely upon simplistic series solutions for more complicated flows. In that case, more sophisticated solution methods would be needed to find v_x and v_y.

3. Transport

3.1. Governing equations

Analyte transport is governed by the two-dimensional (2-D) convection–diffusion equation

$$\frac{\partial \tilde{C}}{\partial \tilde{t}} = \tilde{D}\left(\frac{\partial^2 \tilde{C}}{\partial \tilde{x}^2} + \frac{\partial^2 \tilde{C}}{\partial \tilde{y}^2}\right) - \left(\tilde{u}_{\tilde{x}}\frac{\partial \tilde{C}}{\partial \tilde{x}} + \tilde{u}_{\tilde{y}}\frac{\partial \tilde{C}}{\partial \tilde{y}}\right), \tag{9}$$

where $\tilde{D}$ is the molecular diffusion coefficient for the system. Because of the symmetry of the flow problem about the $\tilde{y}$-axis, we impose any necessary conditions so this problem is symmetric as well. Once we do so, we can restrict the domain of our problem to

$$0 \le \tilde{x} \le L, \qquad 0 \le \tilde{y}.$$

The boundary conditions at the binding surface $\tilde{y} = 0$ are governed by the reaction. The flux through the surface is equal to the rate of change of the bound receptor concentration, which we denote by $\tilde{B}(\tilde{x}, \tilde{t})$:

$$\tilde{D}\frac{\partial \tilde{C}}{\partial \tilde{y}}(\tilde{x}, 0, \tilde{t}) = \frac{\partial \tilde{B}}{\partial \tilde{t}}. \tag{10a}$$

Note that the flux contains only a diffusive component, because the fluid is motionless at the sensor surface. The introduction of the new unknown $\tilde{B}$ requires the imposition of another boundary condition, which is given by the mass action law. This states that the change in the bound state must be given by a Malthusian dissociation term, as well as a bimolecular production term:

$$\frac{\partial \tilde{B}}{\partial \tilde{t}} = \tilde{k}_{\text{on}}\left[(R_T - \tilde{B})\tilde{C}(\tilde{x}, 0, \tilde{t}) - \tilde{K}\tilde{B}\right], \qquad \tilde{K} = \frac{\tilde{k}_{\text{off}}}{\tilde{k}_{\text{on}}}, \tag{10b}$$

where $\tilde{k}_{\text{on}}$ is the *association rate constant* and $\tilde{k}_{\text{off}}$ is the *dissociation rate constant* for the system. In addition, R_{T} is the concentration of receptor sites, which is assumed to be uniform in $\tilde{x}$, and $\tilde{K}$ is the *affinity* or *equilibrium dissociation constant*.

Next, we choose suitable scales in order to introduce dimensionless variables into (9). Because the diffusion coefficient is small, in most of the device convection is the dominant method of transport. However, from (10a) and the fact that the sensor surface is a streamline, we see that any changes in $\tilde{C}$ at the sensor surface must be caused by diffusion to the surface, which occurs in a thin unstirred Lévêque boundary layer above the sensor. Therefore, as a first choice of dimensionless variable in the $\tilde{y}$-direction we choose y_{v}, the variable for the viscous boundary layer. With this choice, we can directly compare the sizes of the viscous and diffusive boundary layers.

We normalize the concentration of the analyte by the bulk concentration C_{T}, which we assume to be constant. Spatial uniformity arises from the fact that the convective time scale on which the concentration equilibrates is much shorter than the time scales under consideration here. Because the IAsys™ well has a finite volume, temporal uniformity is an appropriate approximation only in the case where much more analyte is available than can possibly bind with all the receptor sites. Otherwise, depletion effects will cause a reduction in the bulk concentration over time.

Given the discussion above, we normalize $\tilde{C}$ by letting

$$C_{\text{v}}(x, y_{\text{v}}, \tilde{t}) = \frac{\tilde{C}(\tilde{x}, \tilde{y}, \tilde{t})}{C_{\text{T}}}. \tag{11}$$

Substituting (11) into (9), we obtain

$$\frac{H}{V}\frac{\partial C_{\text{v}}}{\partial \tilde{t}} = \frac{1}{\text{Sc}\,\text{Re}\,r^2}\frac{\partial^2 C_{\text{v}}}{\partial x^2} + \text{Sc}^{-1}\frac{\partial^2 C_{\text{v}}}{\partial y_{\text{v}}^2} - xf'(y_{\text{v}})\frac{\partial C_{\text{v}}}{\partial x} + f(y_{\text{v}})\frac{\partial C_{\text{v}}}{\partial y_{\text{v}}}, \tag{12}$$

$$\text{Sc} = \frac{\nu}{\tilde{D}} = \frac{\text{viscous effects}}{\text{diffusive effects}},$$

where we have used (1), (3), and (7). Here Sc is the *Schmidt number*, which is very large. Because Re is also much greater than 1, diffusion in the y_{v}-direction dominates.

However, because of the size of Sc, even that diffusion is a secondary effect in the viscous layer. Thus, *another* boundary layer must be introduced, a diffusive layer that is even smaller than the viscous layer. We expect the analyte concentration to evolve in this region, so we create a time scale to achieve a balance in (12). Therefore, we let

$$y = \text{Sc}^{1/3} y_{\text{v}} = \text{Sc}^{1/3}\,\text{Re}^{1/2}\, y_{\text{p}} = \frac{\tilde{y}}{H_D}, \qquad H_D = \frac{H^{1/2}\tilde{D}^{1/3}\nu^{1/6}}{V^{1/2}}, \tag{13a}$$

$$t_D = \frac{V}{H\mathrm{Sc}^{1/3}}\tilde{t} = \frac{V\tilde{D}^{1/3}}{H\nu^{1/3}}\tilde{t}, \qquad C_{\mathrm{v}}(x, y_{\mathrm{v}}, \tilde{t}) = C_D(x, y, t_D). \tag{13b}$$

Here H_D is a typical length scale for diffusion. Because $\mathrm{Sc} \gg 1$, we may expand f and f' using our forms for small arguments in (8). Doing so when substituting (13) into (14), we obtain

$$\frac{\partial C_D}{\partial t_D} = \frac{1}{\mathrm{Sc}^{2/3}\,\mathrm{Re}\, r^2}\frac{\partial^2 C_D}{\partial x^2} + \frac{\partial^2 C_D}{\partial y^2} - 2Fxy\frac{\partial C_D}{\partial x} + Fy^2\frac{\partial C_D}{\partial y}. \tag{14}$$

Clearly, the first term on the right-hand side of (14) is smaller than the other terms, and hence diffusion in the x-direction may be neglected.

We normalize $\tilde{B}$ by the concentration R_{T}, so we have

$$B_D(x, t_D) = \frac{\tilde{B}(\tilde{x}, \tilde{t})}{R_{\mathrm{T}}}. \tag{15}$$

Substituting (15) into (10) and using (13), we obtain

$$\frac{\partial B_D}{\partial t_D} = D\frac{\partial C_D}{\partial y}(x, 0, t_D), \tag{16a}$$

$$\frac{\partial B_D}{\partial t_D} = k_{\mathrm{on}}\big[(1 - B_D)C_D(x, 0, t_D) - KB_D\big], \tag{16b}$$

$$\begin{aligned} D &= \frac{C_{\mathrm{T}}H_D}{R_{\mathrm{T}}} = \frac{\text{analyte available to react}}{\text{receptor sites}}, \\ &= \frac{C_{\mathrm{T}}H^{1/2}\tilde{D}^{1/3}\nu^{1/6}}{R_{\mathrm{T}}V^{1/2}}, \\ k_{\mathrm{on}} &= \frac{\tilde{k}_{\mathrm{on}}C_{\mathrm{T}}H\nu^{1/3}}{V\tilde{D}^{1/3}}, \qquad K = \frac{\tilde{K}}{C_{\mathrm{T}}}. \end{aligned} \tag{17}$$

Combining equations (16), we have the following:

$$\frac{\partial C_D}{\partial y}(x, 0, t_D) = \mathrm{Da}\big[(1 - B_D)C_D(x, 0, t_D) - KB_D\big], \tag{18}$$

$$\begin{aligned} \mathrm{Da} &= \frac{\tilde{k}_{\mathrm{on}}R_{\mathrm{T}}}{\tilde{D}/H_D} = \frac{\text{reaction ``velocity''}}{\text{diffusion ``velocity'' in diffusive boundary layer}} \\ &= \frac{\tilde{k}_{\mathrm{on}}R_{\mathrm{T}}\nu^{1/6}H^{1/2}}{V^{1/2}\tilde{D}^{2/3}}. \end{aligned}$$

Here Da is the *Damköhler number* for the system. Note that as the speed of the reaction slows, $\mathrm{Da} \to 0$. This corresponds to the case where the reaction

is causing very little drain on the flux (see (18)), and, hence, transport to the surface can keep up with the reaction. However, for faster reactions or slower diffusion processes, Da increases, and the effects of transport must be considered.

In the systems we study, one or both of D and Da are small. If D is small, we have immediately from (16a) that the bound state does not evolve on this time scale. If Da is small, then from (18) we see that to leading order the concentration is undisturbed. Because there is no flux into the surface, the reaction cannot proceed. In either case, the evolution of the bound state must occur on a longer time scale.

Any balance must arise in either (16a) or (16b). Following the work in [18], we force a balance in (16b) by letting

$$t = k_{\text{on}} t_D = \tilde{k}_{\text{on}} C_{\text{T}} \tilde{t}, \qquad C_D(x, y, t_D) = C(x, y, t) + o(1), \tag{19a}$$

$$B_D(x, t_D) = B(x, t) + o(1). \tag{19b}$$

Substituting (19) into (16b), we obtain

$$\frac{\partial B}{\partial t} = (1 - B)C(x, 0, t) - KB. \tag{20}$$

Therefore, as indicated by the scaling in (19), it is on the t time scale that the forward reaction occurs. In order for t to represent a longer time scale, $k_{\text{on}} = D\text{Da} \ll 1$, which is true, because we are restricting ourselves to the case where either of those parameters is small.

Substituting (19) into (14) and (16a), we have the following, to leading order:

$$\frac{\partial^2 C}{\partial y^2} = 2Fxy\frac{\partial C}{\partial x} - Fy^2\frac{\partial C}{\partial y}, \qquad 0 \le x \le 1, \quad 0 \le y, \tag{21}$$

$$\frac{\partial C}{\partial y}(x, 0, t) = \text{Da}\frac{\partial B}{\partial t}, \tag{22}$$

where in (21) we have used the fact that k_{on} and Re^{-1} are small. Note that the transport equation is in steady-state form, and hence the analyte evolution is attributable only to the surface reaction, as indicated by (22).

To complete the system, we must introduce additional boundary conditions. For obvious reasons, there must be symmetry about the line $x = 0$, so we have

$$\frac{\partial C}{\partial x}(0, y, t) = 0. \tag{23}$$

As we exit the boundary layer, C must approach the bulk concentration, which has been normalized to 1:

$$C(x, \infty, t) = 1. \tag{24}$$

Last, we must have an initial condition for the bound state, which at this stage we take to be arbitrary:

$$B(x, 0) = B_{\mathrm{i}}(x). \tag{25}$$

Because of the structure of the equations, it is useful to introduce the following transformation:

$$C(x, y, t) = 1 - \mathrm{Da} C_{\Delta}(x, y, t). \tag{26}$$

C_{Δ} thus measures the disturbance in the concentration field because of the surface flux, which is proportional to Da. Substituting (26) into (20)–(24), we obtain

$$\frac{\partial B}{\partial t} = (1 - B)[1 - \mathrm{Da} C_{\Delta}(x, 0, t)] - KB, \tag{27}$$

$$\frac{\partial^2 C_{\Delta}}{\partial y^2} = 2Fxy \frac{\partial C_{\Delta}}{\partial x} - Fy^2 \frac{\partial C_{\Delta}}{\partial y}, \tag{28}$$

$$\frac{\partial C_{\Delta}}{\partial y}(x, 0, t) = -\frac{\partial B}{\partial t}, \tag{29}$$

$$\frac{\partial C_{\Delta}}{\partial x}(0, y, t) = 0, \tag{30}$$

$$C_{\Delta}(x, \infty, t) = 0. \tag{31}$$

The form of the system (27)–(31) is now convenient for various types of analysis.

3.2. Steady state

To gain some insight into the problem, we look at the steady states of equations (27)–(31), which we indicate by the subscript "s". In the steady-state case, the right-hand side of (29) becomes zero, so C_{Δ} obeys an unforced equation with zero boundary conditions. Thus, $C_{\Delta} = 0$. Using this fact in the steady state of (27) and solving, we obtain

$$B_{\mathrm{s}}(x) = \frac{1}{\alpha}, \qquad \alpha = 1 + K. \tag{32}$$

Note that K determines the final bound concentration.

Conversely, for *any* experiment, a measurement of the long-time asymptote of $B_s(x)$ will yield a value for K. Rewriting (32) in dimensional terms, we have

$$B_s(x) = \frac{C_T}{\tilde{K} + C_T}.$$

Thus, by running several experiments with varying values of C_T and graphing B_s versus C_T, one can obtain an estimate for $\tilde{K}$. However, to get an appropriate estimate for both $\tilde{k}_{on}$ and $\tilde{k}_{off}$, we must have another piece of information, which we derive in later sections.

In fact, a nonlinear regression is not necessary. If we take the ratio of the steady-state bound concentration B_s to the injected concentration of unbound ligands, we obtain the following:

$$\frac{B_s}{C_T} = \frac{1}{\tilde{K}} - \frac{B_s}{\tilde{K}}.$$

Therefore, plotting a graph of B_s/C_T versus B_s for various C_T will give $\tilde{K}$ as the negative reciprocal of the slope. Such graphs are called *Scatchard plots* [26].

3.3. Dimensional analysis

We note that the deviation from a uniform value of C is driven by (22). Because the variables are all dimensionless, to leading order the transport effects depend only on Da. (In particular, it will be shown that for small Da, the effects of transport are proportional to Da.) Note that there are two types of parameters in Da: ones that are specific to the device (ν, H, V, and R_T) and ones that are specific to the reaction ($\tilde{k}_{on}$ and $\tilde{D}$).

Therefore, to compare two devices we need calculate only the parameters in Da that are device specific. In particular, using the parameters in the Appendix, we have that for the IAsys^{TM},

$$\mathrm{Da} = \left(6.2 \times 10^{-14} \frac{\mathrm{mol} \cdot \mathrm{s}^{1/3}}{\mathrm{cm}^{5/3}}\right) \frac{\tilde{k}_{on}}{\tilde{D}^{2/3}}.$$

We compare the IAsys^{TM} device with the BIAcore^{TM} measurement device. Based on a similar measurement principle, the BIAcore^{TM} consists of a sensor surface on a channel ceiling. The analyte then flows down the channel in a recirculating loop [18]. Using the parameters from [18] for the BIAcore^{TM}, we obtain

$$\mathrm{Da} = \left(1.06 \times 10^{-13} \frac{\mathrm{mol} \cdot \mathrm{s}^{1/3}}{\mathrm{cm}^{5/3}}\right) \frac{\tilde{k}_{on}}{\tilde{D}^{2/3}}.$$

Because Da is of comparable size for both devices, one might expect that the effects of transport in each are similar. However, in the BIAcore^{TM} there

are two measurement errors associated with transport. As described above for the IAsys^{TM}, there is a *normal error* associated with the fact that the two species are not in equlibrium because of a disparity in time scales. We call this a "normal error," because it depends on the effects of the flux, which acts in the direction normal to the sensor surface.

Second, there is a *transverse error* attributable to the fact that the analyte concentration in the BIAcore^{TM} evolves nonuniformly in space, with a lower analyte concentration downstream as molecules react with binding sites. We call this a "transverse error," because it involves a nonuniformity along the sensor surface. However, we shall see that because of the nature of the stagnation flow presented here, there is no transverse error in this model.

4. Constant initial state

We now consider the case where the initial condition $B_i(x)$ is a constant, which we denote simply by B_i. Because the initial condition is uniform in x, one may ask whether B is independent of x for all time. If so, we see from (27) that C must be uniform in x. The boundary conditions (29)–(31) are independent of x if B is, and, hence, we have a self-consistent *ansatz*.

Because (28) does not include t, we may separate the t- and y-dependences by letting

$$C_\Delta(x, y, t) = \frac{dB}{dt}(t)C_1(y). \tag{33}$$

Substituting (33) into (28), (31), (29), and (27), we obtain

$$\frac{d^2C_1}{dy^2} = -Fy^2\frac{dC_1}{dy}, \qquad C_1(\infty) = 0, \tag{34a}$$

$$\frac{dC_1}{dy}(0) = -1, \tag{34b}$$

$$\frac{dB}{dt} = \frac{1-\alpha B}{1+\mathrm{Da}(1-B)C_1(0)}. \tag{35}$$

We note that (35) is directly analogous to the "effective rate constant" equations in [8, 22], which hold for small Da. However, in this system, the bound state is always independent of x, so equation (35) is *exact*, rather than approximate. It holds for all Da, no matter the size, as long as $D \ll 1$.

Solving (34), we have

$$C_1(y) = \frac{1}{3^{2/3}F^{1/3}}\Gamma\left(\frac{1}{3}, \frac{Fy^3}{3}\right), \tag{36}$$

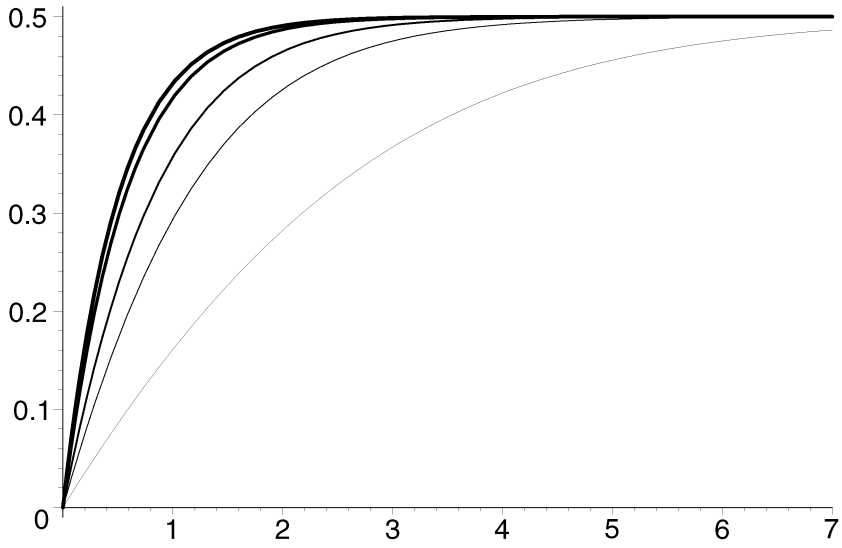

Figure 4. B versus t for $K = 1$ and $B_\mathrm{i} = 0$. In decreasing order of thickness: Da = 0, 0.1, 0.5, 1, 3.

where Γ is the incomplete gamma function. For our purposes, we need only $C_1(0)$, which is given by

$$C_1(0) = \frac{\Gamma(1/3)}{3^{2/3}F^{1/3}}. \tag{37}$$

Substituting (37) into (35), we obtain

$$\frac{dB}{dt} = \frac{1-\alpha B}{1+\gamma(1-B)}, \qquad \gamma = \frac{\mathrm{Da}\Gamma(1/3)}{3^{2/3}F^{1/3}}. \tag{38}$$

Although (38) is the most useful form for analysis, we may solve it to obtain an implicitly defined solution

$$e^{-\gamma(B-B_\mathrm{i})}\left(\frac{1-\alpha B}{1-\alpha B_\mathrm{i}}\right)^{1+\gamma K/\alpha} = e^{-\alpha t}, \tag{39}$$

where we have used (25).

Figure 4 shows a graph of B versus t (as given by (39)) for various values of Da. The thickest line is Da = 0, the case where there are no transport effects at all. Note that as Da increases, the time needed for the bound state to reach equilibrium also increases. This is because increasing Da corresponds to slower transport to the reacting surface, which limits the rate of reaction.

Some discussion of the uniformity in the x-direction is warranted. Because we are considering the special geometry near a stagnation point, v_y is independent of x. This unusual phenomenon allows the uniform solution

presented in this section to develop. (The same phenomenon also keeps the width of the viscous layer independent of x [25].) Because the only dependence on x occurs in the x-velocity, it may be ignored. Physically, exactly enough new ligand is being brought to the surface by the convective stream to replace any taken away during the reaction.

In the true IAsys^{TM} device, v_y must depend on x. For example, note from Figure 2 that even in that diagram, $\partial v_y/\partial x(1, y) = 0$. However, an appreciable portion of the sensor surface is in the neighborhood of the stagnation point, and hence (39) should be a good approximation of the full solution. Nevertheless, for more accurate models of the flow, more sophisticated methods must be used to solve the transport equations. The easiest way to introduce these mathematical techniques is to consider the case where $B_i(x)$ is not constant.

5. Small Da, nonuniform case

5.1. Regular expansion

Now we examine the case where the initial condition is not uniform in x. To preserve the symmetries we exploited in section 3, we require that, although not uniform, the initial condition must be *symmetric* in x. Although we could handle the case where B_i is odd in x, for simplicity, we also require that B_i be even in x.

We specialize to the case of small Da where transport effects are small. To achieve this parameter range, experimentalists should set up their apparatus so that

$$\mathrm{Da} \ll 1 \Longrightarrow V \gg \frac{\tilde{k}_{on}^2 R_T^2 \nu^{1/3} H}{\tilde{D}^{4/3}}.$$

Of course, one must be able to construct an *a priori* estimate for $\tilde{k}_{on}$ to obtain a usable threshold for V. Note that the bound depends on the square of R_T. The higher R_T is, the easier it is to obtain good measurements from the mirror. However, loading up the sensor with receptors will necessitate increasing V to keep Da low. Thus, for R_T large, it may be impossible to increase V such that Da is very close to zero. Finally, we note that the bound in the IAsys^{TM} device is somewhat less sensitive on R_T than the bound for the BIAcore^{TM} device, which depends on R_T^3 [18].

In this case, C_Δ is really the second term in an expansion for C in the (now perturbation) parameter Da. The equivalent series for B is given by

$$B(x, t) = B_0(x, t) + \mathrm{Da} B_1(x, t) + o(\mathrm{Da}). \tag{40}$$

Substituting (40) into (27) and (25), we obtain

$$\frac{\partial B_0}{\partial t} = 1 - \alpha B_0, \qquad B_0(x, 0) = B_{\mathrm{i}}(x), \tag{41a}$$

$$\frac{\partial B_1}{\partial t} = -(1 - B_0)C_{\Delta}(x, 0, t) - \alpha B_1, \qquad B_1(x, 0) = 0. \tag{41b}$$

A brief discussion of the operator in (41a) is appropriate. Rewriting the equation with the parameters and independent variables in dimensional form, we have

$$\frac{\partial B_0}{\partial \tilde{t}} = \tilde{k}_{\mathrm{on}} C_{\mathrm{T}} - \left(\tilde{k}_{\mathrm{on}} C_{\mathrm{T}} + \tilde{k}_{\mathrm{off}}\right) B_0,$$

where we have used (10b), (7), and (19). Therefore, a plot of $\partial B_0/\partial \tilde{t}$ versus B_0 will yield a straight line with slope

$$S = -(\tilde{k}_{\mathrm{on}} C_{\mathrm{T}} + \tilde{k}_{\mathrm{off}}). \tag{42}$$

Because C_{T} is a known quantity that can be varied from experiment to experiment, a graph of S versus C_{T} will be a straight line with slope $\tilde{k}_{\mathrm{on}}$ and intercept $\tilde{k}_{\mathrm{off}}$. Note also that because of the special form of (42), we do not need to use the steady-state solution to provide information about K.

Solving (41a), we obtain

$$B_0(x, t) = \frac{1 - e^{-\alpha t}}{\alpha} + B_{\mathrm{i}}(x) e^{-\alpha t}. \tag{43}$$

Of course, this is the standard type of exponential behavior one would expect. The IAsys™ device does not measure B, but rather the average of B over the sensor surface. In our model system, the width of the device runs from $x = -1/3$ to $x = 1$, so we may define the average as follows:

$$\bar{B}(t) = \frac{3}{4} \int_{-1/3}^{1} B(x, t)\, dx. \tag{44a}$$

However, the flow and initial condition are symmetric about the y-axis, so the true average would be

$$\bar{B}(t) = \frac{3}{4}\left[2 \int_{0}^{1/3} B(x, t)\, dx + \int_{1/3}^{1} B(x, t)\, dx\right]. \tag{44b}$$

If we considered a case where $B(x, t)$ was odd, only the second integral would survive.

Substituting (43) into (44b), we have the following:

$$\bar{B}_0(t) = \frac{1 - e^{-\alpha t}}{\alpha} + \bar{B}_{\mathrm{i}} e^{-\alpha t}. \tag{45}$$

Note that the x- and t-dependences separate in this problem. Therefore, we see that (45) is the solution to the uniform problem (38) with $\mathrm{Da} = 0$ and a uniform initial condition given by $\bar{B}_\mathrm{i}$.

Because our definition of t contains only $\tilde{k}_\mathrm{on}$, it is clear that from this solution (which contains K in α) one can calculate the dimensional rate constants easily. However, (45) holds exactly only in the case where $\mathrm{Da} = 0$. Therefore, we continue by constructing the next order in the perturbation expansion. This new expansion will allow improved estimation of parameters in the case where Da is small.

Substituting (40) and (43) into (29), we obtain

$$\frac{\partial C_\Delta}{\partial y}(\xi, 0, t) = -e^{-\alpha t}\big[1 - \alpha B_\mathrm{i}(x)\big]. \tag{46}$$

Therefore, even in the nonuniform case, there exists a uniform component of the flux. Thus, we may decompose our solution into a uniform and nonuniform part. We also note that because of the structure of our problem, the only time dependence in C_Δ must arise through the right-hand side of (46). Therefore, we perform the following substitution:

$$C_\Delta(x, y, t) = e^{-\alpha t}[C_1(y) + C_2(\xi, y)], \qquad \xi = x^{3/2}, \tag{47}$$

where we introduce the variable ξ in order to simplify some algebra. Here C_1 is the solution given by (36).

Substituting (40) into (28), (41b), (31), and (46), we have the following:

$$\frac{\partial^2 C_2}{\partial y^2} = 3F\xi y\frac{\partial C_2}{\partial \xi} - Fy^2\frac{\partial C_2}{\partial y}, \qquad C_2(\xi, \infty) = 0, \tag{48}$$

$$\frac{\partial B_1}{\partial t} = -(1 - B_0)e^{-\alpha t}[C_1(0) + C_2(\xi, 0)] - \alpha B_1 \tag{49a}$$

$$C_2(\xi, 0) = -\frac{e^{\alpha t}}{1 - B_0}\left(\frac{\partial B_1}{\partial t} + \alpha B_1\right) - C_1(0) \equiv g(\xi), \tag{49b}$$

$$\frac{\partial C_2}{\partial y}(\xi, 0) = \alpha B_\mathrm{i}(\xi)H(1 - \xi). \tag{50}$$

Note that in (49b) g is a function only of ξ because the dependence of B_1 on t will be determined totally through its interaction with C_2 in (49a). Substituting (37) into (49b) and solving for B_1, we obtain

$$B_1(x, t) = -e^{-\alpha t}\left\{\frac{1 - e^{-\alpha t}}{\alpha}\left[\frac{1}{\alpha} - B_\mathrm{i}(x)\right] + \frac{tK}{\alpha}\right\}\left[\frac{\Gamma(1/3)}{3^{2/3}F^{1/3}} + g\right]. \tag{51}$$

We now turn our attention to the actual calculation of g. To solve the problem, we extend our domain so that it is semi-infinite in the ξ-direction. We can do this because of the underlying convective nature of the problem, which sweeps information out of the zone $x < 1$. As indicated in section 3.1, any diffusion in the ξ-direction is negligible.

With the new semi-infinite domain in ξ, we may introduce the standard notion of a Mellin transform in the ξ-direction:

$$\mathscr{M}(a) = \hat{a}(\lambda) = \int_0^\infty \xi^{\lambda-1} a(\xi)\, d\xi, \qquad \mathscr{M}^{-1}(\hat{a}) = a(\xi) = \frac{1}{2\pi i}\int_{\mathrm{C}} \hat{a}(\lambda)\xi^{-\lambda}\, d\lambda,$$

where C is the Bromwich contour. Taking the Mellin transform of (48) and (49b), we have

$$\frac{d^2\hat{C}_2}{dy^2} = -3F\lambda y\hat{C}_2 - Fy^2\frac{d\hat{C}_2}{dy}, \tag{52}$$

$$\hat{C}_2(0) = \hat{g}, \tag{53a}$$

$$\hat{C}_2(\infty) = 0. \tag{53b}$$

By introducing the following substitutions:

$$\hat{C}_2(y) = ye^{-\eta}h(\eta), \qquad \eta = \frac{Fy^3}{3},$$

into (52), we obtain

$$\eta\frac{d^2h}{d\eta^2} + \left(\frac{4}{3} - \eta\right)\frac{dh}{d\eta} - (1-\lambda)h = 0. \tag{54}$$

The solutions of (54) are given by the Kummer functions in [27], 13.1. We rewrite the solutions in the $\hat{C}_2$ notation to yield

$$\hat{C}_2 = ye^{-\eta}\big[a_1 M(1-\lambda, 4/3, \eta) + a_2 U(1-\lambda, 4/3, \eta)\big], \tag{55}$$

where a_1 and a_2 are arbitrary constants. Using the asymptotic expansions for the Kummer functions of large argument given in [27], 13.1.4 and 13.1.8, we obtain an expression for $\hat{C}_2$ for large η, which we use in (53b):

$$\lim_{\eta\to\infty} ye^{-\eta}\left[a_1\frac{\Gamma(4/3)}{\Gamma(1-\lambda)}e^{\eta}\eta^{-(1+\lambda)/3} + a_2\eta^{-(1-\lambda)}\right] = 0.$$

Although technically both terms on the right-hand side tend to zero, the first term does so algebraically; whereas, the second term decays exponentially. To match to algebraic decay, the next order term in C_{v} must diverge algebraically as $y_{\mathrm{v}} \to 0$. However, from (12), we again note that there is no diffusion

in the viscous layer. Thus, any singularity in the boundary condition must be convected from upstream. Because there is no such singularity in the problem, we must take $a_1 = 0$.

To satisfy the boundary condition at $y = 0$, we use the asymptotic expansions for the Kummer functions of small argument given in [27], 13.1.3 and 13.1.2. Doing so and using our choice of a_1, we obtain an expression for $\hat{C}_2$ near zero. Then we use this expression in (53a) to obtain the following:

$$a_2 = \frac{\hat{g} F^{1/3} \Gamma(1-\lambda)}{3^{1/3}\Gamma(1/3)}. \tag{56}$$

We proceed by substituting (56) and $a_1 = 0$ into (55) to obtain an expression for $\partial \hat{C}_2/\partial y(0)$, which we can then relate to $\hat{g}$:

$$\hat{g} = -\left[\frac{\Gamma(1/3)}{3^{2/3}F^{1/3}\Gamma(2/3)}\right]\frac{\Gamma(2/3-\lambda)}{\Gamma(1-\lambda)}\frac{\partial \hat{C}_2}{\partial y}(0), \tag{57}$$

where we have used the Mellin transform of (50). Inverting (57) using the formulas in [28], we obtain

$$g(\xi) = -\frac{1}{3^{2/3}F^{1/3}\Gamma(2/3)}\int_0^{\xi}\frac{1}{\xi'}\left(\frac{\xi}{\xi'}-1\right)^{-2/3}\frac{\partial C_2}{\partial y}(\xi', 0)\, d\xi' \tag{58}$$

in the ξ-coordinates, which can be rewritten in the x-coordinates as

$$g(x) = -\frac{3^{1/3}}{2F^{1/3}\Gamma(2/3)}\int_0^x \frac{1}{(x^{3/2}-x'^{3/2})^{2/3}}\frac{\partial C_2}{\partial y}(x', 0)\, dx', \tag{59a}$$

$$= -\frac{3^{1/3}\alpha}{2F^{1/3}\Gamma(2/3)}\int_0^x \frac{B_{\mathrm{i}}(x')}{(x^{3/2}-x'^{3/2})^{2/3}}\, dx', \tag{59b}$$

where in obtaining (59b) we have used (50).

5.2. Remarks on a uniform expansion

Although it seems as if we have found the first two terms in a uniform expansion for B, this is not the case. Expanding (51) for large t, we have the following:

$$B_1 \sim -\frac{e^{-\alpha t}tK}{\alpha}\left[\frac{\Gamma(1/3)}{3^{2/3}F^{1/3}} + g\right], \qquad t \to \infty, \tag{60}$$

which is similar in form to a secular term in a two-timing problem. This is because of the presence of a secular forcing of the operator in (41b). Of course, because B_0 approaches an $O(1)$ steady state, $\mathrm{Da}B_1 \ll B_0$ for all t, and so technically, the expansion does not fail at this order. However, the form of (60) should still give us pause, because if we were to subtract off B_{s},

then for $t = O(\mathrm{Da}^{-1})$, the second term in our expansion would be the same size as the displacement from the steady state.

The standard way to fix the secularity is to introduce a multiple-scale expansion. Because the secularity occurs at first order, the appropriate slow time scale is $\tau = \mathrm{Da}t$. The solution procedure proceeds as above, except that g no longer depends on $B_\mathrm{i}(x)$ as in (59b), but on an amplitude function $a(x, \tau)$, which equals $B_\mathrm{i}(x)$ when $\tau = 0$:

$$g(x, \tau) = -\frac{3^{1/3}}{2F^{1/3}\Gamma(2/3)} \int_0^x \frac{\alpha a(x', \tau)}{(x^{3/2} - x'^{3/2})^{2/3}}\, dx'.$$

To suppress the secularity in (41b), one may use the Mellin transform to obtain the following equation for $\hat{a}$:

$$\frac{\partial \hat{a}}{\partial \tau} + \frac{K}{\alpha}\left\{-\left[\frac{\Gamma(1/3)}{3^{2/3}F^{1/3}\Gamma(2/3)}\right]\frac{\Gamma(2/3 - \lambda)}{\Gamma(1 - \lambda)}(\alpha\hat{a})\right\} = 0.$$

However, we immediately note that the solution of this problem will be an exponential of gamma functions in λ, which does not have an explicit inverse Mellin transform.

Thus, we conclude that this technique, although perhaps theoretically more pleasing, fails to yield a result that is usable in practice. For calculation purposes, we must use the solutions in (43) and (51), but only for $t = o(\mathrm{Da}^{-1})$.

5.3. Particular nonuniformities

Now we examine some special cases of the nonuniform formula. Suppose that in addition to being even in x, $B_\mathrm{i}(x)$ is also analytic. Then it must have a series in powers of $x^{2n} = \xi^{4n/3}$, where n is a non-negative integer. Substituting this form into (50), we obtain

$$\frac{\partial C_2}{\partial y}(\xi, 0) = \alpha\xi^{4n/3}H(1 - \xi). \tag{61}$$

Substituting (61) into (58) and rewriting in terms of x, we have the following:

$$g(x) = -\frac{\Gamma((4n + 2)/3)\Gamma(1/3)}{3^{2/3}F^{1/3}\Gamma(1 + 4n/3)\Gamma(2/3)}(\alpha x^{2n}), \qquad 0 \le x \le 1. \tag{62}$$

Therefore, if forced at some even power of x through $B_\mathrm{i}(x)$, the concentration field responds at the same power of x with the new coefficient in (62). Thus, at any time t, the analyte has the same general structure as it has initially. Hence, there is no transverse error associated with this model. In the case $n = 0$, we obtain

$$g(x) = -\frac{\alpha\Gamma(1/3)}{3^{2/3}F^{1/3}},$$

which exactly matches with (37) once one takes into account the difference between (34b) and (61).

We conclude by illustrating the behavior for a special case; namely, when

$$B_{\mathrm{i}}(x) = 1 - x^2. \tag{63}$$

Substituting (63) into (43) and (45), we immediately obtain $B_0(x, t)$ and its average:

$$B_0(x, t) = \frac{1 + Ke^{-\alpha t}}{\alpha} - x^2 e^{-\alpha t},$$
$$\bar{B}_0(t) = \frac{1 + Ke^{-\alpha t}}{\alpha} - \frac{7}{27} e^{-\alpha t}.$$

In this case, we may use (62) twice to calculate $g(x)$:

$$g(x) = -\frac{\alpha}{3^{2/3} F^{1/3}} \left[\Gamma(1/3) - \frac{9x^2}{4\Gamma(2/3)} \right]. \tag{64}$$

Substituting (63) and (64) into (51), we have the following:

$$B_1(x, t) = \frac{e^{-\alpha t}}{3^{2/3} F^{1/3}} (a_1 + a_2 x^2)(a_3 + a_4 x^2), \tag{65}$$

$$a_1 = \frac{K}{\alpha}(t - a_2), \qquad a_2 = \frac{1 - e^{-\alpha t}}{\alpha}, \qquad a_3 = K\Gamma(1/3), \qquad a_4 = -\frac{9\alpha}{4\Gamma(2/3)}.$$

The average of (65) is found to be

$$\bar{B}_1 = \frac{e^{-\alpha t}}{3^{2/3} F^{1/3}} \left[a_1 a_3 + \frac{7}{27}(a_2 a_3 + a_1 a_4) + \frac{61 a_2 a_4}{405} \right]. \tag{66}$$

Figure 5 shows a graph of $\bar{B}_1$ versus t in order to indicate the behavior of the correction to $\bar{B}_0$. What is not apparent from the graph (because both decay) is that $|\mathrm{Da}\bar{B}_1| \gg |\bar{B}_0 - B_{\mathrm{s}}|$ as $t \to \infty$, a violation of the assumption of our perturbation expansion. However, note from the graph that the correction is small, even without the Da coefficient.

Because it adds on another layer of complexity, one may ask whether the size of the effect of the spatial variability justifies its inclusion. In other words, what is the error if we use (39) to estimate our solution, but replace B_{i} with the average of the initial condition here, given by $\bar{B}_{\mathrm{i}} = 20/27$?

To answer that question, in Figure 6 we plot the difference between the uniform solution given in (39) with $B_{\mathrm{i}} = 20/27$ and $\bar{B}_0 + \mathrm{Da}\bar{B}_1$. From our discussion in section 5.1 we expect the error to be $O(\mathrm{Da})$, because at leading order the x- and t-dependences separate. Indeed, the linear dependence on Da is easily seen by looking at the peak in the graph. However, we also note that the error in not using the nonuniformity of the initial condition is small.

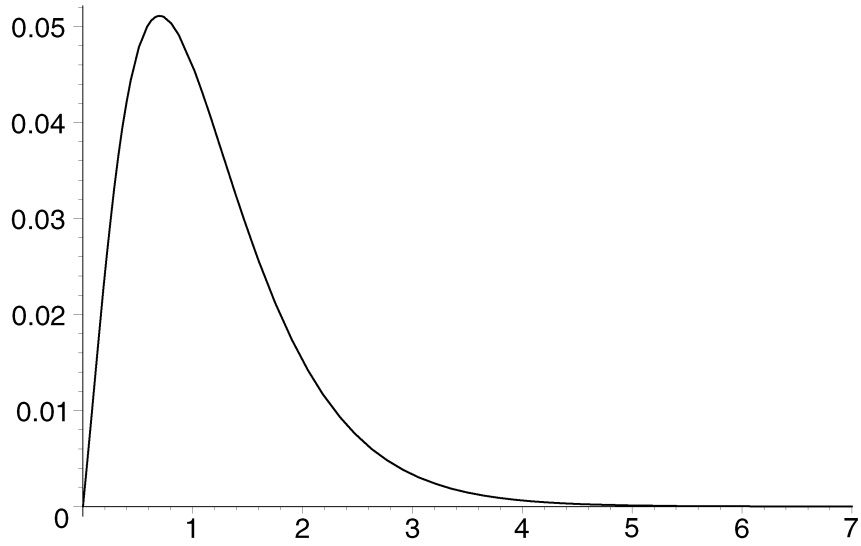

Figure 5. $\bar{B}_1$ versus t for $K = 1$.

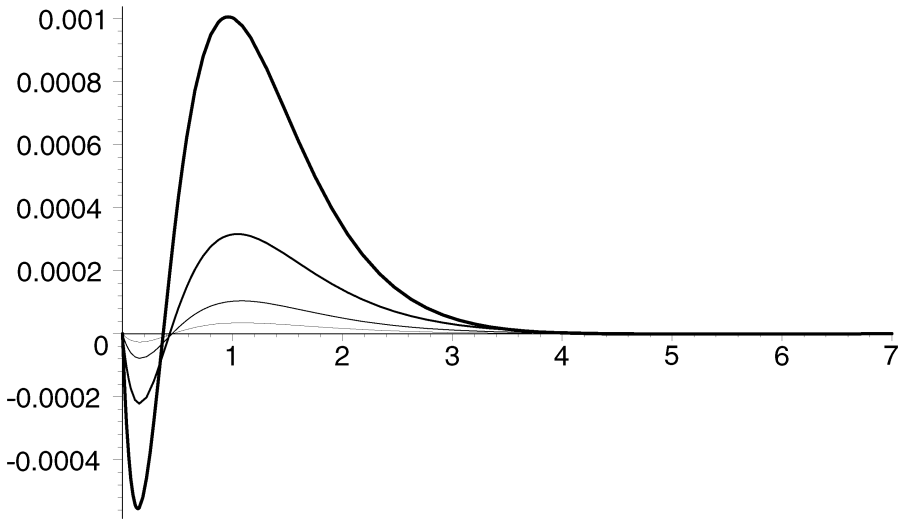

Figure 6. $|B - (\bar{B}_0 + \mathrm{Da}\bar{B}_1)|$ versus t for $K = 1$. In increasing order of thickness: $\mathrm{Da} = 0.005$, 0.015, 0.045, and 0.135.

6. Remarks on moderate Da

As mentioned earlier, if the speed of the reaction is fast enough, there may be no way to keep Da small. Therefore, we discuss briefly the case where $\mathrm{Da} = O(1)$, $D \ll 1$, and the initial state is nonuniform. The solution process

for C_Δ proceeds as in section 5.1, with a few changes. First, solving (27) for $C_\Delta(x, 0, t)$, we obtain

$$C_\Delta(x, 0, t) = \frac{1}{\mathrm{Da}}\left[1 - \frac{1}{1-B}\left(\frac{\partial B}{\partial t} + KB\right)\right] \equiv g(x, t). \tag{67}$$

Equation (67) simply provides a new definition for g. The solution process for C_Δ proceeds as in section 5.1 up through (59a). Then substituting in (29), we have

$$g = \frac{3^{1/3}}{2F^{1/3}\Gamma(2/3)} \int_0^x \frac{1}{(x^{3/2} - x'^{3/2})^{2/3}} \frac{\partial B}{\partial t}(x', t)\, dx'. \tag{68}$$

Equating (67) and (68), we obtain the following:

$$1 - \frac{\partial B}{\partial t} - \alpha B = \frac{3^{1/3}\mathrm{Da}(1-B)}{2F^{1/3}\Gamma(2/3)} \int_0^x \frac{1}{(x^{3/2} - x'^{3/2})^{2/3}} \frac{\partial B}{\partial t}(x', t)\, dx'. \tag{69}$$

In the limit that $\mathrm{Da} \to 0$, (69) reduces to the evolution equation (41a) for B_0, as expected.

In contrast to its counterpart in section 5.1, equation (69) is nonlinear and, hence, difficult to solve. However, one may solve it numerically using techniques similar to those in [23].

7. Conclusions and further research

Scientists must obtain accurate estimates of rate constants for reactions in order to understand the underlying biology and chemistry. The advent of resonant mirror technology and its application in the IAsys^{TM} device allows experimentalists to measure the concentration of bound ligands accurately in real time. However, the correct analysis of the data necessitates the formulation of mathematical models that incorporate the important effects in the system.

In this work, we presented a model for the IAsys^{TM} device. By far the most complicated aspect of the system is the flow field, and we expect that a correct solution of the entire field would necessitate a numerical solution. Although we simplified the intricate flow dynamics down to simple 2-D stagnation flow, we expect our results to be qualitatively correct, because much of the sensor surface is in the neighborhood of the stagnation point.

The full transport model includes convection, diffusion, and reaction at the sensor surface. Using the special case of stagnation flow, we found that if B is initially uniform in x, it will remain so for all time. This is because the concentration C of the analyte also remains independent of x. However, because this uniformity is a direct result of the choice of stagnation flow, we

analyzed cases where B_i was not uniform in x in order to gain insight into the evolution with more realistic flow fields.

The key dimensionless group in the problem is the Damköhler number Da. The limiting case $\mathrm{Da} \to 0$ corresponds to the total separation of the transport and reaction processes. If Da is small but nonzero, transport effects play a role. We derived the first-order correction to the bound-state concentration in the case where B_i depends on x. The correction can be used only for times $t = o(\mathrm{Da}^{-1})$, after which the solution exhibits a secularity. Although we derived the first term in a multiple-scale expansion and identified the relevant second time scale ($\mathrm{Da}t$), the equation has no explicit solution.

In the case of larger Da, the solution can be expressed in terms of a nonlinear integral equation that must be solved numerically. One area of further research is to use the techniques outlined in [23] to solve the resulting integral equation. As in section 5.3, a key avenue to pursue is the error induced by using the uniform solution (39) instead of the solution to the full problem.

In addition to providing improved estimates to the rate constants in selected situations, the careful modeling and scaling in sections 2 and 3 provide a sturdy mathematical framework for further studies. There are several interesting areas for such studies. Clearly, one area of interest must be the consideration of more realistic flows in the IAsys^{TM}.

Also, in contrast to the BIAcore^{TM}, which consists of a recirculating channel of analyte, in the IAsys^{TM}, a fixed amount of analyte is placed in the well at the start of the experiment. If this amount is not much greater than the amount of analyte used up when the reaction is complete, then depletion effects arise [13, 29]. These effects will change the matching condition (24) and hence the solution. In particular, we expect the reaction to slow as the analyte is depleted.

Last, in many applications, the receptors are embedded in a thin (200–500 nm) dextran layer on the sensor surface, rather than attached to the sensor surface itself [12]. Thus, the true system in this case is a set of coupled diffusion equations, one for the bulk flow and one for the dextran layer. If the thickness of the layer is negligible, our approximation of a surface boundary condition is appropriate. However, we note in the Appendix that the thickness of the dextran layer is only an order of magnitude smaller than a typical value of H_D. Clearly, a perturbation approach would yield important information about the effects of such a layer.

8. Nomenclature

8.1. Variables and parameters

Units are listed in terms of length (L), mass (M), moles (N), or time (T). If the same letter appears both with and without tildes, the letter with a tilde has

dimensions; whereas, the letter without a tilde is dimensionless. The equation where a quantity first appears is listed, if appropriate.

a: arbitrary constant or function, variously defined

$\tilde{B}(\tilde{x}, \tilde{t})$: bound ligand concentration on surface $\tilde{y} = 0$ at position $\tilde{x}$ and time $\tilde{t}$, units N/L^2

C: Bromwich contour

$\tilde{C}(\tilde{x}, \tilde{y}, \tilde{t})$: unbound ligand concentration at position $(\tilde{x}, \tilde{y})$ and time $\tilde{t}$, units N/L^3

$\tilde{D}$: molecular diffusion coefficient, units L^2/T (9)

Da: the Damköhler number, which measures the ratio of reaction and diffusion effects

F: constant of proportionality in Falkner–Skan solution, defined as $f''(0)/2$ (8)

$f(y_v)$: Falkner–Skan solution for boundary-layer velocity (7a)

$g(\cdot)$: Dirichlet condition on C_2 at $y = 0$ (49b)

H: typical height scale, units L

$h(\eta)$: function used in nonuniform solution

$\tilde{K}$: affinity (or dissociation equilibrium) constant for system, defined as $\tilde{k}_{\text{off}}/\tilde{k}_{\text{on}}$, units N/L^3 (10b)

$\tilde{k}_{\text{off}}$: dissociation rate constant, units T^{-1} (10b)

$\tilde{k}_{\text{on}}$: binding rate constant, units $L^3/(NT)$ (10b)

L: distance of stirrer from external wall, units L

$\mathscr{M}$: Mellin transform

n: integer exponent (61)

R_T: receptor site density on surface, units N/L^2 (15)

r: aspect ratio, defined as L/H (6a)

Re: Reynolds number for the system, defined as VH/ν

S: slope of a line (42)

Sc: Schmidt number for the system, defined as $\nu/\tilde{D}$ (12)

$\tilde{t}$: dimensional time, units T (9)

$\tilde{u}(\tilde{x}, \tilde{y})$: fluid velocity at position $(\tilde{x}, \tilde{y})$, units L/T

V: velocity of stirrer, units L/T

$v(x, y_v)$: dimensionless velocity at position (x, y_v) in the viscous boundary layer (3a)

$\tilde{x}$: measurement in direction parallel to reacting surface, units L

$\tilde{y}$: measurement in direction perpendicular to reacting surface, units L

Z: integers

8.2. Greek

α: dimensionless parameter, defined in (32) as $1 + K$
γ: dimensionless parameter, defined in (38) as $\mathrm{Da}\Gamma(1/3)/3^{2/3}F^{1/3}$
ξ: scaled variable, defined as $x^{3/2}$ (47)
η: distorted y variable, value $F\eta^3/3$
λ: variable in Mellin transform space
ν: kinematic viscosity of fluid (3b)
τ: long-time scale in multiple-scale expansion

8.3. Other notation

D: as a subscript, used to indicate the diffusive time scale (13a)
i: as a subscript on B, used to indicate the initial state
$n \in Z$: as a subscript on a or C, merely an index (33); as a subscript on B, indicates a series in Da (40)
p: as a subscript, used to indicate potential flow scalings (1)
s: as a subscript, used to indicate a steady state (32)
T: as a subscript, used to indicate the total value of a quantity (11)
v: as a subscript, used to indicate the viscous boundary layer (3a)
$\tilde{x}$: as a subscript, used to indicate velocity in the $\tilde{x}$-direction
$\tilde{y}$: as a subscript, used to indicate velocity in the $\tilde{y}$-direction
Δ: as a subscript on C, used to indicate a displacement from a constant state (26)
$\bar{}$: used to denote the mean of the bound concentration over the reacting strip, defined in (44a) as

$$\bar{B}(t) = \frac{3}{4}\int_{-1/3}^{1} B(x, t)\, dx.$$

$\hat{}$: used to indicate the Mellin transform
$'$: on a dependent variable, used to indicate differentiation (7a); on an independent variable, used to indicate a dummy variable of integration (58)

Appendix

We begin by considering the properties of the IAsys^{TM} itself. (These numbers were provided by Jim Ladine of Affinity Sensors [14].) The vibrostirrer oscillates at 140 Hz with a maximum amplitude of 0.5 mm. It is usually run at 85% of that, so we have a typical value for V of 37.4 cm/s.

We assume that the rest position of the vibrostirrer is 0.75 mm above the surface, although this may actually be somewhat too large. We impose

Table 1
Parameter Values from the Literature

	Material Parameters		
Parameter	Lower Bound	Value Used	Upper Bound
$C_T\,(10^{-11}\ \text{mol/cm}^3)$	0.25 [30]	5 [14]	40 [30]
$\tilde{D}\,(10^{-7}\ \text{cm}^2/\text{s})$	2.8 [31]	2.8	10 [30]
$\tilde{k}_{on}\,(10^8\ \text{cm}^3/(\text{mol}\cdot\text{s}))$	6.5×10^{-3} [32]	2.1 [33]	100 [21]
$R_T\,(10^{-12}\ \text{mol/cm}^2)$	0.25 [30]	3 [14]	4 [30]
	Calculated Quantities		
Parameter	Lower Bound	Value Used	Upper Bound
D		2.27×10^{-3}	14.2
Da	4.62×10^{-7}	3.06×10^{-1}	4.48×10^4
$H_D\,(10^{-4}\ \text{cm})$		1.36	3.56
Sc	2×10^3	3.57×10^4	

symmetry upon the flow in the device. This implies that the vibrostirrer, which we model as a jet, is 0.75 mm from the side of the device. Therefore, we have $L = H = 7.5 \times 10^{-2}$ cm, which implies that $r = 1$.

We consider the solution containing the analyte to be water, so we have from [1] that $\nu = 10^{-2}\ \text{cm}^2/\text{s}$, which implies that the Reynolds number is 280. Thus, we may take $\text{Re} \gg 1$ and use laminar inviscid flow theory, because turbulence does not ensue until Re is around 2100 [1].

Ranges for the other material parameters are listed in Table 1, along with the appropriate references. The value used for $\tilde{D}$ is for fibrinogen. The variation in C_T reflects the fact that one can run experiments using different values to create more data sets to increase accuracy. It should be noted that the values in [30] are those for the BIAcore™ device, but they still provide good upper and lower bounds for the IAsys™ device. We note from the table that $D = O(1)$ only in extreme cases and is usually much smaller. Therefore, our use of the t variable as a slow variable in (19) is justified.

Acknowledgments

Many of the calculations herein were checked using Maple. The author thanks Jim Ladine for his helpful discussions regarding the IAsys™ device. This work was supported by the University of Delaware Research Foundation.

References

1. R. B. Bird, W. E. Stewart, and E. N. Lightfoot, *Transport Phenomena*, Wiley, New York, 1960.
2. Y. F. Wang and R. Pollard, An approach for modeling surface-reaction kinetics in chemical vapor deposition processes, *J. Electrochem. Soc*. 142:1712–1725 (1995).
3. P. Duverneuil and J. P. Couderc, Two-dimensional modeling of low-pressure chemical vapor deposition hot wall tubular reactors. 1. Hypotheses, methods, and first results, *J. Electrochem. Soc*. 139:296–304 (1992).
4. M. Michaelidis and R. Pollard, Analysis of chemical vapor deposition of boron, *J. Electrochem. Soc*. 131:860–868 (1984).
5. K. F. Jensen, Modeling of chemical vapor deposition reactors for the fabrication of microelectronic devices, in *Chemical and Catalytic Reactor Modeling*, ACS, Washington, 1984.
6. G. Eigenberger, Modeling and simulation in industrial chemical reaction engineering, in *Modeling of Chemical Reaction Systems*, Springer-Verlag, Heidelberg, 1981.
7. A. Szabo, L. Stolz, and R. Granzow, Surface plasmon resonance and its use in biomolecular interaction analysis (BIA), *Curr. Opin. Struct. Bio*. 5:699–705 (1995).
8. D. A. Edwards, Biochemical reactions on helical structures, *SIAM J. Appl. Math*., in press (2000).
9. B. Goldstein and M. Dembo, Approximating the effects of diffusion on reversible reactions at the cell surface: Ligand-receptor kinetics, *Biophys. J*. 68:1222–1230 (1995).
10. M. Raghavan, M. Y. Chen, L. N. Gastinel, and P. J. Bjorkman, Investigation of the interaction between the class I MHC-related Fc receptor and its immunoglobulin ligand, *Immunity* 1:303–315 (1994).
11. P. E. Buckle, R. J. Davies, T. Kinning, D. Yeung, P. R. Edwards, D. Pollardknight, and C. R. Lowe, The resonant mirror: A novel optical sensor for direct sensing of biomolecular interactions. 2. Applications, *Biosen. Bioelec*. 8:355–363 (1993).
12. P. R. Edwards, A. Gill, D. V. Pollardknight, M. Hoare, P. E. Buckle, P. A. Lowe, and R. J. Leatherbarrow, Kinetics of protein–protein interactions at the surface of an optical biosensor, *Anal. Biochem*. 231:210–217 (1995).
13. P. R. Edwards, C. H. Maule, R. J. Leatherbarrow, and D. J. Winzor, Second-order kinetic analysis of IAsys biosensor data: Its use and applicability, *Anal. Biochem*. 263:1–12 (1998).
14. J. Ladine, Affinity Sensors, June 24, 1999, private communication.
15. R. Karlsson, H. Roos, L. Fägerstam, and B. Persson, Kinetic and concentration analysis using BIA technology, *Methods* 6:99–110 (1994).
16. V. T. Turitto and H. R. Baumgartner, Platelet deposition on subendothelium exposed to flowing blood: Mathematical analysis of physical parameters, *Trans. Amer. Soc. Artif. Int. Org*. 21:593–601 (1975).
17. D. J. O'Shannessy, Determination of kinetic rate and equilibrium binding constants for macromolecular interactions: A critique of the surface plasmon resonance literature, *Curr. Opin. Biotech*. 5:65–71 (1994).
18. D. A. Edwards, Estimating rate constants in a convection-diffusion system with a boundary reaction, *IMA J. Appl. Math*. 63:89–112 (1999).

19. D. BASMADJIAN and M. V. SEFTON, A model of thrombin inacativation in heparinized and nonheparinized tubes with consequences for thrombus formation, *J. Biomed. Mat. Res*. 20:633–651 (1986).

20. T. A. MORTON, D. G. MYSZKA, and I. M. CHAIKEN, Interpreting complex binding kinetics from optical biosensors: A comparison of analysis by linearization, the integrated rate equations, and numerical integration, *Anal. Biochem*. 227:176–185 (1995).

21. D. G. MYSZKA, Kinetic analysis of macromolecular interactions using surface plasmon resonance biosensors, *Curr. Opin. Biotech*. 8:50–57 (1997).

22. D. A. EDWARDS, B. GOLDSTEIN, and D. S. COHEN, Transport effects on surface-volume biological reactions, *J. Math. Bio*., 39:533–561 (1999).

23. D. A. EDWARDS and S. A. JACKSON, Testing the validity of the effective rate constant approximation for surface reaction with transport, *Appl. Math. Let.* submitted.

24. D. J. ACHESON, *Elementary Fluid Dynamics*, Clarendon, Oxford, UK, 1990, 127.

25. L. G. LEAL, *Laminar Flow and Convective Transport Processes: Scaling Principles and Asymptotic Analysis*, Butterworth-Heinemann, Boston, 1992.

26. H. MOTULSKY, *The GraphPad Guide to Analyzing Radioligand Binding Data*, GraphPad Software, San Diego, 1996.

27. M. ABRAMOWITZ and I. A. STEGUN, *Handbook of Mathematical Functions with Formulas, Graphs, and Mathematical Tables*, National Bureau of Standards, Washington, DC, 1972.

28. O. I. MARICHEV, *Handbook of Integral Transforms of Higher Transcendental Functions: Theory and Algorithmic Tables*, Ellis-Horwood, Chichester, UK, 1983.

29. D. R. HALL, N. N. GORGANI, J. G. ALTIN, and D. J. WINZOR, Theoretical and experimental considerations of the pseudo-first-order approximation in conventional kinetic analysis of IAsys biosensor data, *Anal. Biochem*. 253:145–155 (1997).

30. M. L. YARMUSH, D. B. PATANKAR, and D. M. YARMUSH, An analysis of transport resistance in the operation of BIAcore^{TM}; Implications for kinetic studies of biospecific interactions, *Molec. Immun*. 33:1203–1214 (1996).

31. B. K. LOK, Y.-L. CHENG, and C. R. ROBERTSON, Protein adsorption on crosslinked polydimethyl-siloxane using total internal reflection fluorescence, *J. Coll. Int. Sci*. 91:104–116 (1983).

32. W. CHEN, S. KHILKO, J. FECONDO, D. H. MARGULIES, and J. MCCLUSKEY, Determinant selection of major histocompatibility complex class I-restricted antigenic peptides is explained by class I-peptide affinity and is strongly influenced by nondominant anchor residues, *J. Exper. Med*. 180:1471–1583 (1994).

33. M. CORR, A. E. SLANETZ, L. F. BOYD, M. T. JELONEK, S. KHILKO, B. K. AL-RMAADI, Y. S. KIM, S. E. MAHER, A. L. M. BOTHWELL, and D. H. MARGULIES, T cell receptor-MHC class I peptide interactions: Affinity, kinetics, and specificity, *Science* 265:946–949 (1994).

UNIVERSITY OF DELAWARE

(Received August 19, 1999)